Chemical Science

ROYAL SOCIETY OF CHEMISTRY

EDGE ARTICLE

View Article Online
View Journal | View Issue



Cite this: *Chem. Sci.*, 2025, **16**, 9311

All publication charges for this article have been paid for by the Royal Society of Chemistry

# Platinum–copper nanowire networks with enhanced CO tolerance toward methanol oxidation electrocatalysis†

Shiyue Xing,[a] Zhongliang Liu,[a] Yingfang Jiang,[a] Pinghui Tang,[a] Jian Zhang,[a] Jiatang Chen,[b] Huihui Li*[a] and Chunzhong Li*[a]

Developing platinum-based electrocatalysts with high CO tolerance for the methanol oxidation reaction (MOR) is crucial for the practical application of direct methanol fuel cells (DMFCs). Herein, we employed a straightforward one-step method to synthesize $Pt_xCu_y$ network nanowires (NWNs), which exhibit the advantages of structural stability and bimetallic ensembles. The synergistic effect of compressive strain and the ligand effect, induced by Cu incorporation, can effectively lower the d-band center of Pt, thereby weakening the adsorption strength of CO on the catalyst surface. The optimized $Pt_{42}Cu_{58}$ NWNs deliver a peak mass activity of 1.33 A $mg_{Pt}^{-1}$ and a specific activity of 4.43 mA $cm^{-2}$ for the MOR, which are 3.03 and 4.03 times higher than those of commercial Pt/C, respectively. The CO stripping and *in situ* Fourier transform infrared spectroscopy results indicate their high anti-CO poisoning ability and methanol activation capacity. Moreover, the $Pt_{42}Cu_{58}$ NWNs also exhibit an excellent stability with high current densities observed after 3600 s of operation due to the enhanced CO tolerance and the stable three-dimensional (3D) network structure. This work provides a feasible strategy to suppress CO poisoning during the MOR and obtain highly efficient anode catalysts with enhanced durability in the DMFC field.

Received 24th January 2025
Accepted 15th April 2025

DOI: 10.1039/d5sc00656b

rsc.li/chemical-science



## 1 Introduction

Direct methanol fuel cells (DMFCs) represent a promising electrochemical power source, particularly in view of the usage of liquid methanol, which offers advantages in terms of convenience and security for transportation and storage through the existing gasoline infrastructure, as compared to hydrogen.[1] Nevertheless, the sluggish kinetics of the methanol oxidation reaction (MOR), which entails six electron transfer steps at the anode, hinders the progress of DMFCs.[2,3] During the stepwise dehydrogenation of methanol, carbonyl intermediates, particularly CO, tend to strongly adsorb onto the catalyst surface, blocking active sites for follow-up reactions.[4,5] Platinum (Pt) nanoparticle electrocatalysts are presently recognized as the most effective anode catalysts.[1,6,7] However, their catalytic efficiency is significantly hindered by the poisoning effect of the CO intermediate and Ostwald ripening during the MOR process.[5,8–10]

The introduction of late transition metals (LTMs, such as Fe,[11] Co,[12] Ni[13] and Cu[14]) into active Pt sites has emerged as a significant strategy to enhance the accelerated removal of CO. Incorporating LTMs enables the modification of the electronic structure of Pt and induces compressive strain on its surface, which results from the relatively smaller lattice constants of LTMs compared to those of Pt. Both the strain and ligand effects generated in the alloy can finely tune the d-band center, thereby reducing the adsorption strength of CO* intermediates on Pt active sites.[15–20] Moreover, LTMs are abundant in nature and cost-effective, which can significantly reduce the expense of platinum-based catalysts, making them a more viable option for the MOR. Ultrathin one-dimensional nanowires (1D NWs), characterized by a typical diameter of less than 5 nm, exhibit distinctive properties such as high aspect ratios and enhanced atomic utilization efficiency.[21] The NWs can readily self-assemble into a three-dimensional (3D) network structure, characterized by a large surface area with abundant exposed active sites, enhanced conductivity, and a stable structure that resists Ostwald ripening and degradation during the reaction.[22] Therefore, adjusting the d-band center and enhancing structural stability are crucial for designing high-performance catalysts with superior anti-CO poisoning capabilities.

By comparing with Fe,[23] Ni,[24] Co,[25] *etc.*, the Cu incorporation can optimize the d-band center to achieve an optimal balance between reduced CO binding energy and enhanced OH

[a]*Key Laboratory for Ultrafine Materials of Ministry of Education, School of Chemical Engineering, East China University of Science and Technology, Shanghai 200237, China. E-mail: huihuili@ecust.edu.cn; czli@ecust.edu.cn*

[b]*Cornell High Energy Synchrotron Source, Wilson Laboratory, Cornell University, Ithaca, New York 14853, USA*

† Electronic supplementary information (ESI) available. See DOI: https://doi.org/10.1039/d5sc00656b

adsorption.[26,27] The integration of Cu doping strategies with the distinctive structural advantages of NWs offers a promising approach for the design of MOR catalysts. Significant advancements have been achieved in PtCu NW systems. For instance, Zhang *et al.* synthesized screw thread-like Pt–Cu NWs featuring high-index facets, which provided an abundance of catalytically active sites and consequently enhanced the intrinsic catalytic activity.[28] Other researches also demonstrated that the construction of atomic steps[29] and the controlled introduction of surface defects[26,29,30] can effectively increase active site density on NW surfaces, thereby boosting MOR performance. However, the critical role of composition-dependent strain–ligand synergy in optimizing CO tolerance and enhancing MOR activity remains underestimated. A more thorough investigation of this regulatory mechanism could reveal new avenues for the design of high-performance MOR catalysts.

Herein, we employed a simple one-step method to introduce Cu into Pt active sites, forming $Pt_xCu_y$ NW networks (NWNs) for the MOR. The characterization and *in situ* experimental results demonstrate that the synergistic effects of compressive strain and ligand effects, induced by Cu incorporation, can reduce CO adsorption, enhance CO oxidation, and liberate Pt active sites. This promotes MOR activity and improves resistance to CO poisoning. The optimized $Pt_{42}Cu_{58}$ NWNs demonstrate a peak mass activity (MA) of 1.33 A $mg_{Pt}^{-1}$ and specific activity (SA) of 4.43 mA $cm^{-2}$ for the MOR, 4.03 times and 5.03 times that of commercial Pt/C, respectively. Moreover, the $Pt_{42}Cu_{58}$ NWNs exhibit excellent stability with high current densities observed after 3600 s of continuous operation attributed to their superior resistance to CO poisoning and the stable 3D NWN structure.

## 2 Results and discussion

### 2.1 Synthesis and characterization

The $Pt_xCu_y$ alloy NWNs were synthesized *via* a simple one-step method, as illustrated in Fig. 1a, using $H_2PtCl_6$ and $CuCl_2 \cdot 2H_2O$ as metal precursors, sodium borohydride as a strong

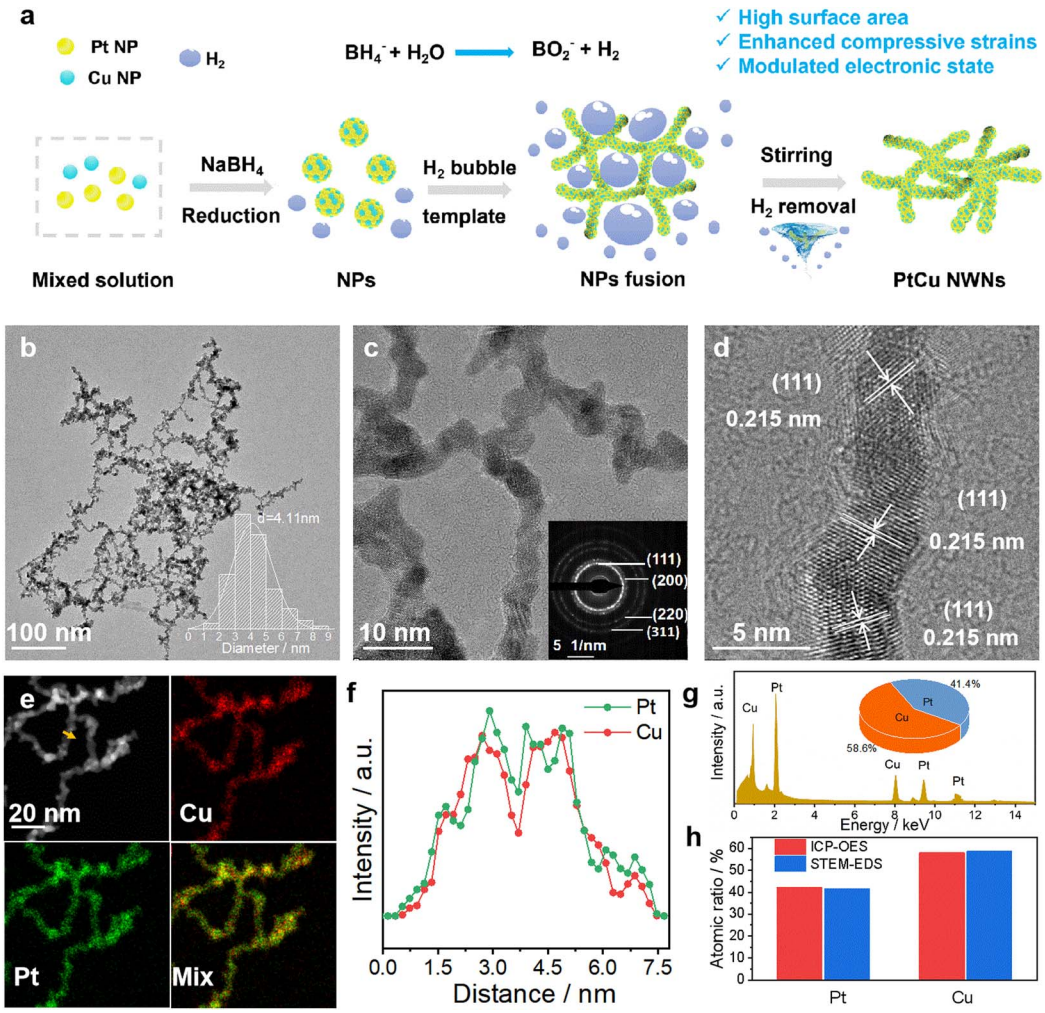


Fig. 1 (a) Schematic illustration of the preparation of $Pt_xCu_y$ NWNs. Structural and compositional characterization of $Pt_{42}Cu_{58}$ NWNs. Representative (b) low- and (c) high-magnification TEM images (inset shows the corresponding SAED pattern). (d) HRTEM image. (e) HAADF-STEM image and STEM-EDS elemental mappings. (f) Line-scanning profiles across the yellow arrow shown in (e). (g) STEM-EDS spectra. (h) The atomic ratio of $Pt_{42}Cu_{58}$ NWNs characterized by STEM-EDS and ICP-OES.

reducing agent, and the *in situ* generated hydrogen as the dynamic template for the formation of 1D structures[31] (details in the Experimental section in the ESI†). In this synthesis, the addition of sodium borohydride at low temperatures is crucial in controlling the kinetics of nucleation and growth of NWs. Replacement with another strong reducing agent, such as $N_2H_4 \cdot H_2O$, would result in the formation of nano-dendrites rather than NWs (Fig. S1†), due to the lack of the dynamic template of hydrogen. And the increase in temperature would lead to the formation of low-quality NWNs, due to the accelerated nanoparticle assembly (Fig. S2†).

The morphology of $Pt_{42}Cu_{58}$ NWNs obtained from the scanning electron microscopy (SEM) in Fig. S3† and the low-magnification transmission electron microscope (TEM) in Fig. 1b reveal a 3D porous nano-network structure, which is primarily composed of interconnected wavy 1D NWs with a diameter of approximately 4.1 nm. The selected-area electron diffraction (SAED) pattern (inset of Fig. 1c) officially defines the polycrystalline nature of $Pt_{42}Cu_{58}$ NWNs. The detailed structural characterization of these NWs was further conducted using high-resolution transmission electron microscopy (HRTEM). HRTEM images reveal that the lattice spacing of the $Pt_{42}Cu_{58}$ NWNs is 0.215 nm, which is smaller than that of the surface cubic platinum (fcc) at 0.226 nm. This observation indicates the formation of an alloy structure with lattice contraction, as shown in Fig. 1d. The (111) crystal planes on the surface of NWNs are not oriented in parallel, which may lead to the development of wavy structures. The homogeneous distribution of Pt and Cu elements throughout the whole $Pt_{42}Cu_{58}$ NWN surface was observed in the STEM-EDX elemental mapping images (Fig. 1e). The EDS line-scanning analysis, conducted along the direction indicated by the yellow arrows in Fig. 1e (as shown in Fig. 1f), demonstrated a uniform distribution of Pt and copper Cu. In addition, the atomic ratio of Pt to Cu, as determined by STEM-EDS, was 41.4 : 58.6, which is in agreement with the results obtained from inductively coupled plasma-optical emission spectrometry (ICP-OES) measurements (42.0 : 58.0). Overall, the aforementioned results provide compelling evidence for the successful synthesis of ultrathin cross-linked $Pt_{42}Cu_{58}$ NWNs. The catalysts featuring analogous structures but varying Pt/Cu ratios as control samples were also successfully synthesized by adjusting the molar ratio of the two metal precursors. The morphology of the NWNs and the corresponding atomic ratios are presented in Fig. S4–S6 and Table S1.†

### 2.2 Strain and ligand effects

To investigate the phase and electronic structure of the prepared $Pt_xCu_y$ NWNs, X-ray diffraction (XRD), X-ray

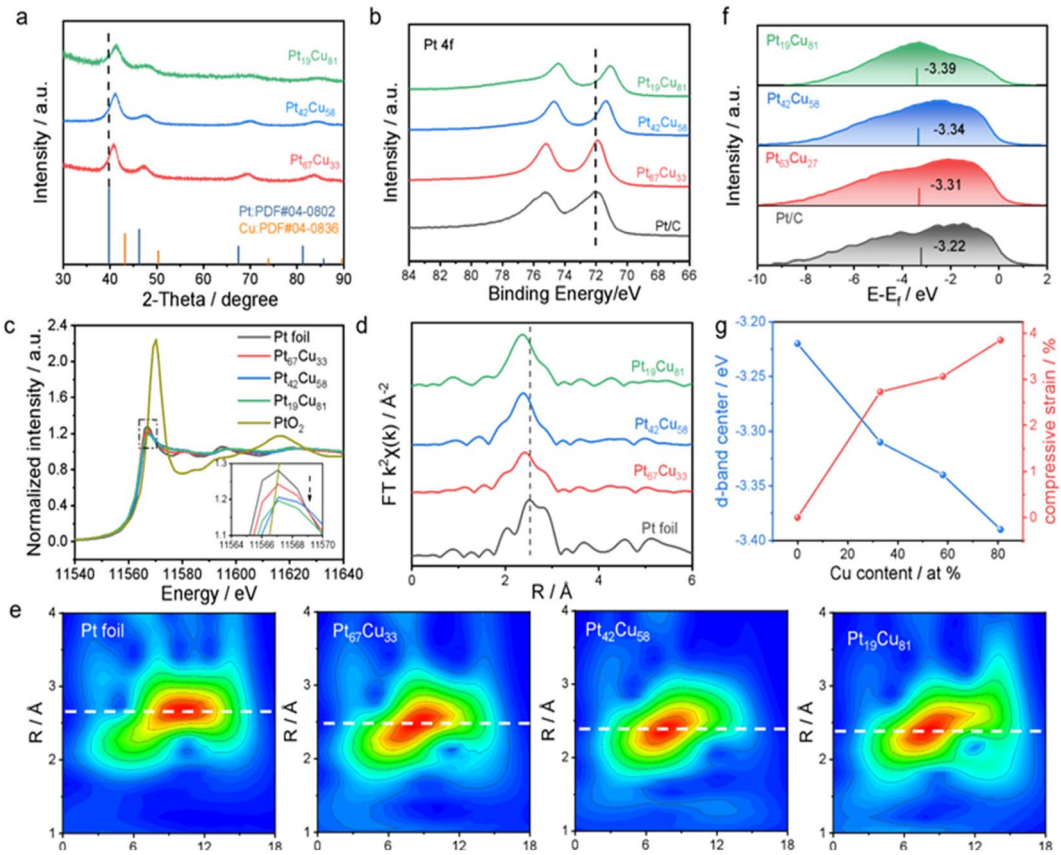


Fig. 2 Characterization of $Pt_xCu_y$ NWNs. (a) XRD pattern of $Pt_xCu_y$ NWNs. (b) High-resolution XPS spectra of Pt 4f for $Pt_xCu_y$ NWNs and commercial Pt/C. (c) Normalized Pt $L_3$-edge XANES spectra of $Pt_xCu_y$ NWNs, $PtO_2$, and Pt foil, respectively. (d) FT-EXAFS spectra of $Pt_xCu_y$ NWNs and Pt foil. (e) Wavelet transform (WT) plots of $Pt_xCu_y$ NWNs and Pt foil, respectively. (f) Surface valence band photoemission spectra of $Pt_xCu_y$ NWNs and commercial Pt/C. (g) Evolution of the d-band center and lattice strain as a function of Cu content in $Pt_xCu_y$ NWNs.

photoelectron spectroscopy (XPS), and X-ray adsorption fine structure (XAFS) were carried out. The XRD diffraction peaks of $Pt_xCu_y$ NWNs with different compositions (Fig. 2a) show a typical fcc polycrystalline structure and are located between the standard diffraction spectra of Pt metal (JCPDS card no. 04-0802) and Cu (JCPDS card no. 04-0836), indicating the formation of a PtCu binary alloy. The diffraction peak positions shift to higher angles with increasing Cu content relative to pure Pt, further confirming the presence of compressive strain due to lattice mismatch between Pt and the smaller atomic radius Cu. As shown in Table S2,† the compressive strains induced in the Pt (111) lattice of $Pt_{67}Cu_{33}$, $Pt_{42}Cu_{58}$, and $Pt_{19}Cu_{81}$ are 2.73%, 3.06%, and 3.85%, respectively.[32–35]

XPS analysis revealed the electron transfer from Cu to Pt due to the difference in electronegativity (Fig. 2b and S10†). As shown in Fig. 2b, the binding energy of the Pt 4f peak shifts negatively with lower electronegativity Cu doping and that of $Pt_{42}Cu_{58}$ NWNs demonstrates a 0.69 eV negative shift compared to commercial Pt/C (Fig. S10†), which can lower the platinum d-band center for the increased number of filled orbitals.[18,36] Concurrently, the Cu 2p spectra (Fig. S11†) reveal a gradual positive shift in binding energy with higher Cu content, confirming a reduction in electron density of Cu atoms. This complementary trend in binding energy for Pt 4f and Cu 2p directly validates the electron donation from Cu to Pt. Besides, we can also find that most of the Pt and Cu on the surface of $Pt_{42}Cu_{58}$ were in the metallic state (Fig. S10†), demonstrating the formation of the alloy.

Fig. 2c presents the normalized Pt $L_3$-edge X-ray absorption near-edge structure (XANES) spectra of $Pt_xCu_y$ NWNs compared with Pt foil and $PtO_2$. They exhibit a high degree of similarity to that of Pt foil, with a notable divergence from that of $PtO_2$, demonstrating the Pt is mainly in a metallic state.[37,38] As previously reported, the intensity of the white line is proportional to the transition of electrons from the Pt $2p_{3/2}$ core to the 5d state, and it can be used as an indicator of the electron occupancy of the Pt 5d band.[20] A lower white line peak intensity is observed in $Pt_xCu_y$ NWNs compared to that in Pt foil. By integrating the Pt $L_3$-edge white line areas,[39,40] we quantified the 5d band holes (vacancies) as 0.785, 0.771, and 0.745 for $Pt_{67}Cu_{33}$, $Pt_{42}Cu_{58}$, and $Pt_{19}Cu_{81}$, respectively, systematically lower than those of pure Pt (1.000) and demonstrating a Cu-dependent reduction trend (Fig. S7, S8 and Table S3†). This progressive decline in 5d vacancies signifies enhanced electron density within the Pt 5d orbitals upon Cu incorporation, corroborating our XPS findings. This electron enrichment lowers the Pt d-band center, thereby weakening adsorbate binding strength.[36] The Fourier transform extended XAFS (EXAFS) (Fig. 2d) and its fitting results (Fig. S9 and Table S3†) clearly confirmed the coordination environment of the Pt $L_3$ edge for the catalysts. As shown in Fig. 2d, the $k^2$-weighted EXAFS for $Pt_xCu_y$ NWNs at Pt $L_3$-edge without phase correction shows a lower scattering peak ($Pt_{67}Cu_{33}$ at 2.479 Å, $Pt_{42}Cu_{58}$ at 2.446 Å, and $Pt_{19}Cu_{81}$ at 2.402 Å) in contrast to Pt foil (2.632 Å), which could be assigned to the Pt–Pt/Cu paths, confirming that the $Pt_xCu_y$ NWNs predominantly exhibit shortened Pt–M (M = Pt/Cu) metal bonds. This observation indicates the formation of the PtCu alloy structure with lattice contraction. Meanwhile, the fitting results in Table S3† can also prove the existence of Pt–Pt and Pt–Cu bonds in the PtCu NWWs. For instance, the main metal bonds are the Pt–Cu bond with a coordination number of 4.1 and the Pt–Pt bond with a coordination number of 5.0 in $Pt_{42}Cu_{58}$ NWNs (Table S4†). There are no Pt–O bonds in the $Pt_xCu_y$ NWNs compared to $PtO_2$, which is also visually confirmed by the wavelet transform (WT) (Fig. 2e and S12†). Furthermore, it is noteworthy that the bond length of the Pt–M bond (about 2.65–2.72 Å) in $R$ space has been shortened with more Cu content involved in comparison to the Pt–Pt bond (2.77 Å) in Pt foil from the EXAFS and WT analysis, demonstrating the compressive strain involved, which is in agreement with the HRTEM and the XRD results.[41] The compressive strain can broaden the d-band and then downshift the d-band center, resulting from the increasing orbital overlap in Pt atoms after smaller metal atoms are involved.[42,43]

Prior research has demonstrated that a negative shift in the d-band center can weaken the binding energy between the catalyst surface and adsorbates.[44,45] The findings illustrated above indicate that $Pt_xCu_y$ NWNs, which exhibit a rich-electron Pt surface and existing compressive strain, can synergistically decrease the d-band center, causing it to deviate from the Fermi level. Therefore, the XPS valence band spectrum of the catalysts was measured and analyzed (Fig. 2f). The results show that the d-band center positions of the compressive strained $Pt_{67}Cu_{33}$ NWNs, $Pt_{42}C_{58}$ NWNs, and $Pt_{19}Cu_{81}$ NWNs have decreased by 0.09 eV, 0.12 eV, and 0.17 eV, respectively, compared to that of Pt/C, suggesting that Cu incorporation leads to a downward shift in the d-band center, which may enhance the MOR activity by weakening the binding force between the Pt-based catalysts and the carbonyl intermediate species adsorbed on the surface. Furthermore, a significant positive correlation was observed among the compressive strain, the d-band center, and the Cu content (Fig. 2g). This indicates that an increase in Cu content corresponds to a greater compressive strain and a lower d-band center. Thus, the compressive strain and d-band electrons can be effectively tuned by merely modifying the Cu content, allowing for the regulation of intermediate adsorption strength and the optimization of catalyst performance for the MOR.

### 2.3 Electrocatalytic performances of the $Pt_xCu_y$ NWNs

The MOR activity and stability of the obtained $Pt_xCu_y$ NWNs and commercial Pt/C were evaluated under acid conditions. The details of the tests were in the Experimental section in the ESI.† The electrochemically active surface area (ECSA) was measured by CV in acid electrolyte at 50 mV $s^{-1}$ (Fig. 3a). The calculated ECSA values for $Pt_{67}Cu_{33}$, $Pt_{42}Cu_{58}$, $Pt_{19}Cu_{81}$, and commercial Pt/C are 29.12, 30.09, 33.10, and 37.75 $m^2$ $g_{Pt}{}^{-1}$, respectively. Besides, the ECSA values of the three $Pt_xCu_y$ NWNs are comparable to those of Pt/C, indicating that the 3D nanonetworks with ultrathin NWs could effectively expose active sites and improve atomic utilization.

The MOR curves of catalysts were recorded in an acid electrolyte containing methanol (see Fig. 3b and c). As illustrated in Fig. 3d, the $Pt_{42}Cu_{58}$ NWNs demonstrate the highest mass

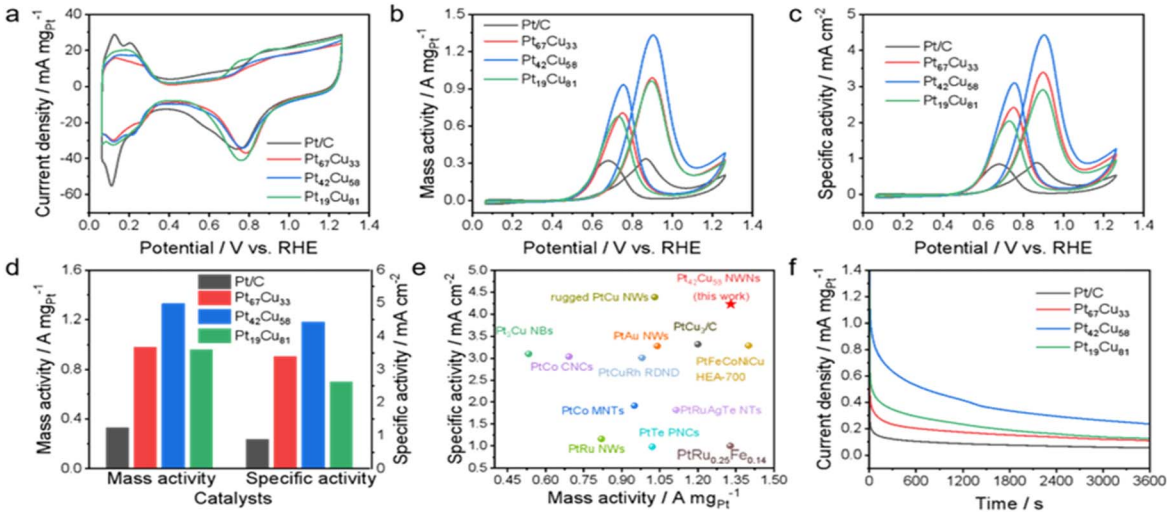


Fig. 3 Electrocatalytic performances of $Pt_xCu_y$ NWNs and commercial Pt/C for the MOR. (a) CV curves of the catalysts recorded in $N_2$-saturated 0.1 M $HClO_4$ electrolyte at a scan rate of 50 mV $s^{-1}$. (b) Pt mass-normalized and (c) ECSA-normalized MOR curves measured in 0.1 M $HClO_4$ containing 0.5 M methanol solution at a scan rate of 50 mV $s^{-1}$. (d) Histogram of MOR mass activities and specific activities of the corresponding catalysts. (e) Comparison of MOR activities of other reported Pt-based electrocatalysts. (f) *I*–*t* curves from the chronoamperometric tests in 0.1 M $HClO_4$ containing 0.5 M methanol solution.

activity (MA, 1.33 A $mg_{Pt}^{-1}$), which is 1.36, 1.39, and 4.03 times higher than those of $Pt_{67}Cu_{33}$ NWNs (0.98 A $mg_{Pt}^{-1}$), $Pt_{19}Cu_{81}$ NWNs (0.96 A $mg_{Pt}^{-1}$), and commercial Pt/C (0.33 A $mg_{Pt}^{-1}$), respectively. Furthermore, the specific activity (SA, 4.43 mA $cm^{-2}$) of $Pt_{42}Cu_{58}$ NWNs obtained by normalizing the ECSA is also higher than those of $Pt_{67}Cu_{33}$ NWNs (3.39 mA $cm^{-2}$), $Pt_{19}Cu_{81}$ NWNs (2.63 mA $cm^{-2}$), and commercial Pt/C (0.88 mA $cm^{-2}$), respectively. A significant volcano-type dependence on MOR activity was observed, influenced by the Cu component, compressive strain, and the position of the d-band center (Fig. S13†). The MOR activity of $Pt_{42}Cu_{58}$ NWNs is compared with that of previously reported Pt-based catalysts, as illustrated in Fig. 3d and summarized in Table S5.† The enhanced MOR activity may be attributed to the optimized electron structure of Pt, which has been tuned by strain and ligand effects after Cu doping and the presence of enriched active sites for the ultrathin 3D structure.

The catalytic stability was evaluated through chronoamperometry (CA) tests. As illustrated in Fig. 3d, the current densities for $Pt_{42}Cu_{58}$ NWNs remained superior to those of the other catalysts throughout the 3600 s CA tests. The structural change of $Pt_{42}Cu_{58}$ NWNs was negligible, except for a slight widening of the lattice stripes from 0.215 nm to 0.218 nm, which may result from the unavoidable leaching of Cu atoms during the reaction process (Fig. S14†). In contrast, the activity of Pt/C was poor, accompanied by severely damaged morphology due to CO poisoning and severe aggregation of the nanoparticles (Fig. S15†). The electrochemical tests above demonstrate that the excellent MOR catalytic activity and stability of $Pt_{42}Cu_{58}$ NWNs can be attributed to the robust CO tolerance after Cu doping and its advanced 3D structure.

To achieve a deeper understanding of the catalysts' activity, a series of kinetic studies were undertaken. Linear sweep voltammetry (LSV) measurements were conducted in acidic methanol media. As shown in Fig. S16a and b,† $Pt_{42}Cu_{58}$ NWNs have the lowest onset potential and Tafel slope (80.45 mV $dec^{-1}$) compared to the other catalysts, indicating their enhanced MOR kinetics. As shown in Fig. S16c and Table S6,† $Pt_{42}Cu_{58}$ NWNs also possess the highest values of $j_0$ and $\alpha$, both of which are calculated from the Tafel equation, demonstrating accelerated electron transfer.[46] The electrochemical impedance spectroscopy (EIS) analysis was further performed, as shown in Fig. S16d.† The impedance arc diameter of the $Pt_{42}Cu_{58}$ NWNs is significantly smaller compared to that of the other catalysts, indicating a lower charge transfer resistance and enhanced kinetic activity. These findings are in agreement with the previously mentioned results. Additionally, LSV curves at various scan rates were obtained for all samples (Fig. S17†). The plots of current density *versus* the square root of the scan rate for all electrocatalysts demonstrate a linear relationship, suggesting a diffusion-limited process.[47] The $Pt_{42}Cu_{56}$ NWNs show the highest slope of 0.52, demonstrating accelerated mass/electron transfer.[46] Finally, we also obtained LSV profiles at different temperatures to investigate the thermodynamics of the MOR for all samples. Fig. S18† illustrates the linear relationship between the current density $\ln j$ and $1/T$ for all the samples. The corresponding apparent activation energy values ($E_a$) calculated from the slope value of the Arrhenius plot can reflect the adsorption energy of methanol and intermediate species on the catalyst surface.[48] The $Pt_{42}Cu_{58}$ NWNs show the smallest value of $E_a$ (39.93 kJ $mol^{-1}$) compared to the other catalysts, indicating that methanol oxidation is more facile for $Pt_{42}Cu_{58}$ NWNs.[49] In brief, $Pt_{42}Cu_{58}$ NWNs that achieve an optimal balance between the strain and ligand effects can substantially reduce the energy barrier and enhance the kinetics of the MOR.

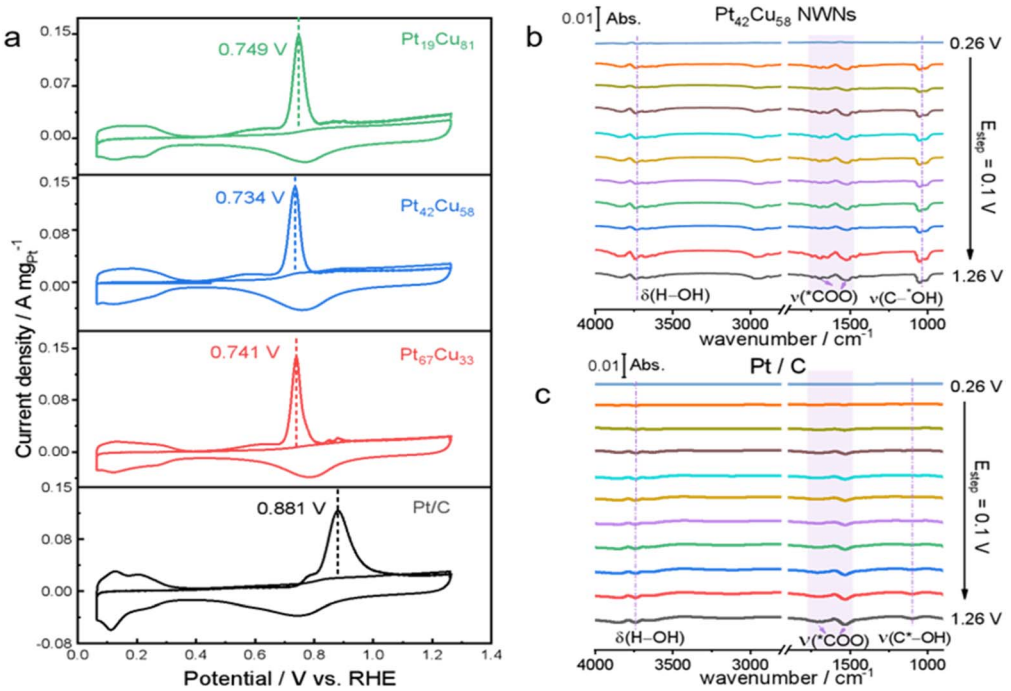


Fig. 4 (a) CO stripping tests of $Pt_xCu_y$ NWNs and commercial Pt/C. (b) Electrochemical *in situ* ATR-FTIR spectrum of the MOR on $Pt_{42}Cu_{58}$ NWNs and (c) Pt/C.

### 2.4 Anti-CO poisoning ability of the $Pt_xCu_y$ NWNs

To further explore the anti-CO poisoning ability of $Pt_{42}Cu_{58}$ NWNs in the enhancement of MOR performance, we employed CO stripping and *in situ* attenuated total reflectance Fourier transform infrared (ATR-FTIR) spectroscopy. CO is a key intermediate in the MOR process.[50] As shown in Fig. 4a, the CO stripping peak potentials for all $Pt_xCu_y$ alloys shift negatively in comparison to commercial Pt/C (0.881 V *vs.* RHE), indicating improved CO oxidation capabilities and increased resistance to CO poisoning. Notably, the $Pt_{42}Cu_{58}$ NWNs (0.734 V *vs.* RHE) display a lower peak potential than the $Pt_{19}Cu_{81}$ NWNs (0.749 V *vs.* RHE) and $Pt_{19}Cu_{81}$ NWNs (0.741 V *vs.* RHE), suggesting that a moderate downshift in the d-band center is crucial for facilitating the removal of CO and enhancing the capacities for CO tolerance.

ATR-FTIR spectroscopy was further used to detect the adsorbed species at the molecular level on the optimized $Pt_{42}Cu_{58}$ NWNs and commercial Pt/C for comparison (Fig. 4b and c). We can find featured bonds like the stretching vibration C–*OH (about 1022 $cm^{-1}$) and the antisymmetric stretching vibration *COO (from 1500 to 1630 $cm^{-1}$), which belong to methanol and the intermediate *COOH, respectively.[5,51,52] With the potential improved, those bonds appeared first at 0.36 V in $Pt_{42}Cu_{58}$ NWNs, 100 mV lower than that of commercial Pt/C (0.46 V), implying the high methanol activation capacity of $Pt_{42}Cu_{58}$ NWNs. The stretching bonds O–H (about 3700 $cm^{-1}$) detected in the two samples may be assigned to OH* from the water dissociation,[53] which can oxidize the CO* to form *COOH and then dehydrogenate to $CO_2$.[14] The combined results of CO stripping and *in situ* ATR demonstrate that the $Pt_{42}Cu_{56}$ NWNs exhibit a high anti-CO poisoning ability and methanol activation capacity. This may be attributed to the weak adsorption of CO on Pt sites, which facilitates the removal of CO and then the liberation of active sites, thereby promoting methanol activation.

## 3 Conclusions

In conclusion, we designed a kind of compressive strained $Pt_{42}Cu_{58}$ NWN with enhanced catalytic activity and robust anti-CO poisoning capacity for the MOR. The experiments demonstrated that the synergy of compressive strain and the ligand effect endowed the catalysts with a downward shifted d-band center, which can weaken the CO adsorption strength on the Pt surface. The optimized $Pt_{42}Cu_{58}$ NWNs achieve a high MOR mass activity of 1.33 A $mg_{Pt}^{-1}$ and specific activity of 4.43 mA $cm^{-2}$, which are 4.03 and 5.03 times higher than those of Pt/C, respectively. The CO striping and *in situ* ATR-FTIR results further indicate their enhanced CO tolerance ability and methanol activation capacity. Moreover, the $Pt_{42}Cu_{58}$ NWNs exhibit excellent stability with high current densities observed after 3600 s of continuous operation attributed to their superior resistance to CO poisoning and the stable 3D NWN structure. This work provides a feasible strategy to suppress CO poisoning during methanol oxidation electrocatalysis and obtain highly efficient anode catalysts with enhanced durability in the DMFC field.

## Data availability

All data generated or analyzed during this study are included in this article and the ESI.†

## Author contributions

All of the authors contributed to the manuscript preparation. Shiyue Xing, Huihui Li and Chunzhong Li conceived the outline of the manuscript. Shiyue Xing, Huihui Li and Chunzhong Li wrote the original draft of the manuscript. Zhongliang Liu, Yingfang Jiang, Pinghui Tang, Jian Zhang, and Jiatang Chen discussed and helped revise the manuscript.

## Conflicts of interest

There are no conflicts to declare.

## Acknowledgements

This work was supported by the National Natural Science Foundation of China (U22B20143, U24A20546, and 22478121), the Shanghai Municipal Science and Technology Major Project, and the Science and Technology Commission of Shanghai Municipality (22dz1205900).

## References

1 J. Wang, B. Zhang, W. Guo, L. Wang, J. Chen, H. Pan and W. Sun, Toward Electrocatalytic Methanol Oxidation Reaction: Longstanding Debates and Emerging Catalysts, *Adv. Mater.*, 2023, **35**, 2211099.

2 H. Li, Y. Pan, D. Zhang, Y. Han, Z. Wang, Y. Qin, S. Lin, X. Wu, H. Zhao, J. Lai, B. Huang and L. Wang, Surface oxygen-mediated ultrathin PtRuM (Ni, Fe, and Co) nanowires boosting methanol oxidation reaction, *J. Mater. Chem. A*, 2020, **8**, 2323–2330.

3 F. Lyu, M. Cao, A. Mahsud and Q. Zhang, Interfacial engineering of noble metals for electrocatalytic methanol and ethanol oxidation, *J. Mater. Chem. A*, 2020, **8**, 15445–15457.

4 A. R. Poerwoprajitno, L. Gloag, J. Watt, S. Cheong, X. Tan, H. Lei, H. A. Tahini, A. Henson, B. Subhash, N. M. Bedford, B. K. Miller, P. B. O'Mara, T. M. Benedetti, D. L. Huber, W. Zhang, S. C. Smith, J. J. Gooding, W. Schuhmann and R. D. Tilley, A single-Pt-atom-on-Ru-nanoparticle electrocatalyst for CO-resilient methanol oxidation, *Nat. Catal.*, 2022, **5**, 231–237.

5 A. Xu, T. Liu, D. Liu, W. Li, H. Huang, S. Wang, L. Xu, X. Liu, S. Jiang, Y. Chen, M. Sun, Q. Luo, T. Ding and T. Yao, Edge-Rich Pt-O-Ce Sites in $CeO_2$ Supported Patchy Atomic-Layer Pt Enable a Non-CO Pathway for Efficient Methanol Oxidation, *Angew. Chem., Int. Ed.*, 2024, **63**, e202410545.

6 M. Zhou, C. Li and J. Fang, Noble-Metal Based Random Alloy and Intermetallic Nanocrystals: Syntheses and Applications, *Chem. Rev.*, 2021, **121**, 736–795.

7 L. Huang, X. Zhang, Q. Wang, Y. Han, Y. Fang and S. Dong, Shape-Control of Pt–Ru Nanocrystals: Tuning Surface Structure for Enhanced Electrocatalytic Methanol Oxidation, *J. Am. Chem. Soc.*, 2018, **140**, 1142–1147.

8 L. Hui, D. Yan, X. Zhang, H. Wu, J. Li and Y. Li, Halogen Tailoring of Platinum Electrocatalyst with High CO Tolerance for Methanol Oxidation Reaction, *Angew. Chem., Int. Ed.*, 2024, **63**, e202410413.

9 R. Chen, Z. Wang, S. Chen, L. Wang, W. Wu, Y. Zhu and N. Cheng, Optimizing Intermediate Adsorption on Pt Sites via Triple-Phase Interface Electronic Exchange for Methanol Oxidation, *Inorg. Chem.*, 2024, **63**, 4364–4372.

10 G. Bai, C. Liu, Z. Gao, B. Lu, X. Tong, X. Guo and N. Yang, Atomic Carbon Layers Supported Pt Nanoparticles for Minimized CO Poisoning and Maximized Methanol Oxidation, *Small*, 2019, **15**, 1902951.

11 Q. Yang, S. Zhang, F. Wu, L. Zhu, G. Li, M. Chen, A. Pei and Y. Feng, Efficient and stable PtFe alloy catalyst for electrocatalytic methanol oxidation with high resistance to CO, *J. Energy Chem.*, 2024, **90**, 327–336.

12 B. Y. Xia, H. B. Wu, N. Li, Y. Yan, X. W. D. Lou and X. Wang, One-Pot Synthesis of Pt-Co Alloy Nanowire Assemblies with Tunable Composition and Enhanced Electrocatalytic Properties, *Angew. Chem., Int. Ed.*, 2015, **54**, 3797–3801.

13 T. Xia, K. Zhao, Y. Zhu, X. Bai, H. Gao, Z. Wang, Y. Gong, M. Feng, S. Li, Q. Zheng, S. Wang, R. Wang and H. Guo, Mixed-Dimensional Pt–Ni Alloy Polyhedral Nanochains as Bifunctional Electrocatalysts for Direct Methanol Fuel Cells, *Adv. Mater.*, 2023, **35**, 2206508.

14 Y. Sun, S. Zhang, S. Sun, L. Wu, J. Tian, Y. Wu, Y. Chen and X. Liu, Cu Tailoring Pt Enables Branched-Structured Electrocatalysts with High Concave Surface Curvature Toward Efficient Methanol Oxidation, *Small*, 2023, **20**, 2307970.

15 S. Chen, N. Liu, J. Zhong, R. Yang, B. Yan, L. Gan, P. Yu, X. Gui, H. Yang, D. Yu, Z. Zeng and G. Yang, Engineering Support and Distribution of Palladium and Tin on MXene with Modulation of the d-Band Center for CO-resilient Methanol Oxidation, *Angew. Chem., Int. Ed.*, 2022, **61**, e202209693.

16 T. Singha, S. Tomar, S. Das and B. Satpati, D-Band Engineering in Pd-Based Nanowire Networks for Further Enhancement in Ethanol Electrooxidation Reaction, *Small Methods*, 2024, **8**, 2400368.

17 V. R. Stamenkovic, B. S. Mun, M. Arenz, K. J. Mayrhofer, C. A. Lucas, G. Wang, P. N. Ross and N. M. Markovic, Trends in electrocatalysis on extended and nanoscale Pt-bimetallic alloy surfaces, *Nat. Mater.*, 2007, **6**, 241–247.

18 J. Chen, F. Zhang, M. Kuang, L. Wang, H. Wang, W. Li and J. Yang, Unveiling synergy of strain and ligand effects in metallic aerogel for electrocatalytic polyethylene terephthalate upcycling, *Proc. Natl. Acad. Sci. U.S.A.*, 2024, **121**, e2318853121.

19 Y. He, Y. Chen, R. Wu, Z. Xiao, M. Li, C. Shi and L. Wang, Ligand effect in surface atomic sites of group VI B transition metals on ultrathin Pt nanowires for enhanced oxygen reduction, *Nano Res.*, 2024, **17**, 5298–5304.

20 L. Tao, K. Wang, F. Lv, H. Mi, F. Lin, H. Luo, H. Guo, Q. Zhang, L. Gu, M. Luo and S. Guo, Precise synthetic control of exclusive ligand effect boosts oxygen reduction catalysis, *Nat. Commun.*, 2023, **14**, 6893.

21 H. Xu, H. Shang, C. Wang and Y. Du, Ultrafine Pt-Based Nanowires for Advanced Catalysis, *Adv. Funct. Mater.*, 2020, **30**, 2000793.
22 Q. Shao, K. Lu and X. Huang, Platinum Group Nanowires for Efficient Electrocatalysis, *Small Methods*, 2019, **3**, 1800545.
23 Y. Nie, X. Qi, R. Wu, R. Yang, H. Wang, M. Deng, S. Zhang, S. Lu, Z. Gu and X. Liu, Structurally ordered PtFe intermetallic nanocatalysts toward efficient electrocatalysis of methanol oxidation, *Appl. Surf. Sci.*, 2021, **569**, 151004.
24 X. Chen, J. Zhao, J. Lian and X. Wang, Achieving superior methanol oxidation electrocatalytic performance by surface reconstruction of PtNi nanoalloys during acid etching process, *Green Chem.*, 2023, **25**, 3198–3207.
25 S. Papadimitriou, S. Armyanov, E. Valova, A. Hubin, O. Steenhaut, E. Pavlidou, G. Kokkinidis and S. Sotiropoulos, Methanol Oxidation at Pt–Cu, Pt–Ni, and Pt–Co Electrode Coatings Prepared by a Galvanic Replacement Process, *J. Phys. Chem. C*, 2010, **114**, 5217–5223.
26 K. Wang, D. Huang, Y. Guan, F. Liu, J. He and Y. Ding, Fine-Tuning the Electronic Structure of Dealloyed PtCu Nanowires for Efficient Methanol Oxidation Reaction, *ACS Catal.*, 2021, **11**, 14428–14438.
27 H. Q. Pham and T. T. Huynh, Platinum–Copper Bimetallic Nanodendritic Electrocatalyst on a $TiO_2$-Based Support for Methanol Oxidation in Alkaline Fuel Cells, *ACS Appl. Nano Mater.*, 2021, **4**, 4983–4993.
28 N. Zhang, L. Bu, S. Guo, J. Guo and X. Huang, Screw Thread-Like Platinum–Copper Nanowires Bounded with High-Index Facets for Efficient Electrocatalysis, *Nano Lett.*, 2016, **16**, 5037–5043.
29 D. Fang, L. Wan, Q. Jiang, H. Zhang, X. Tang, X. Qin, Z. Shao and Z. Wei, Wavy PtCu alloy nanowire networks with abundant surface defects enhanced oxygen reduction reaction, *Nano Res.*, 2019, **12**, 2766–2773.
30 N. Guo, H. Xue, A. Bao, Z. Wang, J. Sun, T. Song, X. Ge, W. Zhang, K. Huang, F. He and Q. Wang, Achieving Superior Electrocatalytic Performance by Surface Copper Vacancy Defects during Electrochemical Etching Process, *Angew. Chem., Int. Ed.*, 2020, **59**, 13778–13784.
31 L. Liu, L.-X. Chen, A.-J. Wang, J. Yuan, L. Shen and J.-J. Feng, Hydrogen bubbles template-directed synthesis of self-supported AuPt nanowire networks for improved ethanol oxidation and oxygen reduction reactions, *Int. J. Hydrogen Energy*, 2016, **41**, 8871–8880.
32 Y. Zheng, A. S. Petersen, H. Wan, R. Hübner, J. Zhang, J. Wang, H. Qi, Y. Ye, C. Liang, J. Yang, Z. Cui, Y. Meng, Z. Zheng, J. Rossmeisl and W. Liu, Scalable and Controllable Synthesis of Pt-Ni Bunched-Nanocages Aerogels as Efficient Electrocatalysts for Oxygen Reduction Reaction, *Adv. Energy Mater.*, 2023, **13**, 2204257.
33 S. Wang, T. Sheng and Q. Yuan, Low-Pt Octahedral PtCuCo Nanoalloys: "One Stone, Four Birds" for Oxygen Reduction and Methanol Oxidation Reactions, *Inorg. Chem.*, 2023, **62**, 11581–11588.
34 H. Guo, L. Li, Y. Chen, W. Zhang, C. Shang, X. Cao, M. Li, Q. Zhang, H. Tan, Y. Nie, L. Gu and S. Guo, Precise Strain Tuning Boosts Electrocatalytic Hydrogen Generation, *Adv. Mater.*, 2023, **35**, 2302285.
35 K. Peng, N. Bhuvanendran, S. Ravichandran, W. Zhang, Q. Ma, Q. Xu, L. Xing, L. Khotseng and H. Su, Bimetallic $Pt_3Mn$ nanowire network structures with enhanced electrocatalytic performance for methanol oxidation, *Int. J. Hydrogen Energy*, 2020, **45**, 30455–30462.
36 J. T. L. Gamler, H. M. Ashberry, S. E. Skrabalak and K. M. Koczkur, Random Alloyed versus Intermetallic Nanoparticles: A Comparison of Electrocatalytic Performance, *Adv. Mater.*, 2018, **30**, 1801563.
37 Y. Lv, L. Lin, R. Xue, P. Zhang, F. Ma, T. Gan, J. Zhang, D. Gao, X. Zheng, L. Wang, Y. Qin, H. Zhao, Y. Dong, Y. Wang and Y. Zhu, Electronegativity Induced d-Band Center Offset for Pt-Rh Dual Sites in High-Entropy Alloy Boosts Liquid Fuels Electrooxidation, *Adv. Energy Mater.*, 2024, **14**, 2304515.
38 T. Shen, D. Xiao, Z. Deng, S. Wang, L. An, M. Song, Q. Zhang, T. Zhao, M. Gong and D. Wang, Stabilizing Diluted Active Sites of Ultrasmall High-Entropy Intermetallics for Efficient Formic Acid Electrooxidation, *Angew. Chem., Int. Ed.*, 2024, **63**, e202403260.
39 J. Chen, Y. M. Yiu, Z. Wang, D. Covelli, R. Sammynaiken, Y. Z. Finfrock and T.-K. Sham, Elucidating the Many-Body Effect and Anomalous Pt and Ni Core Level Shifts in X-ray Photoelectron Spectroscopy of Pt–Ni Alloys, *J. Phys. Chem. C*, 2020, **124**, 2313–2318.
40 D. Wang, X. Cui, Q. Xiao, Y. Hu, Z. Wang, Y. M. Yiu and T. K. Sham, Electronic behaviour of Au-Pt alloys and the 4f binding energy shift anomaly in Au bimetallics- X-ray spectroscopy studies, *AIP Adv.*, 2018, **8**, 065210.
41 Y. Nie, Y. Sun, B. Song, Q. Meyer, S. Liu, H. Guo, L. Tao, F. Lin, M. Luo, Q. Zhang, L. Gu, L.-M. Yang, C. Zhao and S. Guo, Low-Electronegativity Mn-Contraction of PtMn Nanodendrites Boosts Oxygen Reduction Durability, *Angew. Chem., Int. Ed.*, 2023, **136**, e202317987.
42 D. Wang, Z. Chen, Y.-C. Huang, W. Li, J. Wang, Z. Lu, K. Gu, T. Wang, Y. Wu, C. Chen, Y. Zhang, X. Huang, L. Tao, C.-L. Dong, J. Chen, C. V. Singh and S. Wang, Tailoring lattice strain in ultra-fine high-entropy alloys for active and stable methanol oxidation, *Sci. China Mater.*, 2021, **64**, 2454–2466.
43 K. Xu, L. Liang, T. Li, M. Bao, Z. Yu, J. Wang, S. M. Thalluri, F. Lin, Q. Liu, Z. Cui, S. Song and L. Liu, $Pt_{1.8}Pd_{0.2}CuGa$ Intermetallic Nanocatalysts with Enhanced Methanol Oxidation Performance for Efficient Hybrid Seawater Electrolysis, *Adv. Mater.*, 2024, **36**, e2403792.
44 X. Yang, Y. Wang, X. Tong and N. Yang, Strain Engineering in Electrocatalysts: Fundamentals, Progress, and Perspectives, *Adv. Energy Mater.*, 2022, **12**, 2102261.
45 Q. Yao, Z. Yu, L. Li and X. Huang, Strain and Surface Engineering of Multicomponent Metallic Nanomaterials with Unconventional Phases, *Chem. Rev.*, 2023, **123**, 9676–9717.
46 T. T. Huynh, Q. Huynh, Q. V. Nguyen and H. Q. Pham, Lattice Strain and Composition Effects on the Methanol

Oxidation Performance of Platinum–Ruthenium–Nickel Ternary Nanocatalysts, *Inorg. Chem.*, 2023, **62**, 20477–20487.

47 J. Hu, C. Fang, X. Jiang, D. Zhang and Z. Cui, Ultrathin and Porous 2D PtPdCu Nanoalloys as High-Performance Multifunctional Electrocatalysts for Various Alcohol Oxidation Reactions, *Inorg. Chem.*, 2022, **61**, 9352–9363.

48 T. T. Huynh, Q. Huynh, A. Q. K. Nguyen and H. Q. Pham, Strong Component-Interaction in N-doped 2D $Ti_3C_2T_x$-Supported Pt Electrocatalyst for Acidic Ethanol Oxidation Reaction, *Adv. Sustainable Syst.*, 2025, **9**, 2400995.

49 K. Zhang, H. Wang, J. Qiu, J. Wu, H. Wang, J. Shao, Y. Deng and L. Yan, Multi-dimensional Pt/$Ni(OH)_2$/nitrogen-doped graphene nanocomposites with low platinum content for methanol oxidation reaction with highly catalytic performance, *Chem. Eng. J.*, 2021, **421**, 127786.

50 T. He, W. Wang, F. Shi, X. Yang, X. Li, J. Wu, Y. Yin and M. Jin, Mastering the surface strain of platinum catalysts for efficient electrocatalysis, *Nature*, 2021, **598**, 76–81.

51 L. He, M. Li, L. Qiu, S. Geng, Y. Liu, F. Tian, M. Luo, H. Liu, Y. Yu, W. Yang and S. Guo, Single-atom Mo-tailored high-entropy-alloy ultrathin nanosheets with intrinsic tensile strain enhance electrocatalysis, *Nat. Commun.*, 2024, **15**, 2290.

52 F. Yang, J. Ye, L. Gao, J. Yu, Z. Yang, Y. Lu, C. Ma, Y. J. Zeng and H. Huang, Ultrathin PtNiGaSnMoRe Senary Nanowires with Partial Amorphous Structure Enable Remarkable Methanol Oxidation Electrocatalysis, *Adv. Energy Mater.*, 2023, **13**, 2301408.

53 J. Zhu, L. Xia, R. Yu, R. Lu, J. Li, R. He, Y. Wu, W. Zhang, X. Hong, W. Chen, Y. Zhao, L. Zhou, L. Mai and Z. Wang, Ultrahigh Stable Methanol Oxidation Enabled by a High Hydroxyl Concentration on Pt Clusters/MXene Interfaces, *J. Am. Chem. Soc.*, 2022, **144**, 15529–15538.